Review of Inverse Synthetic Aperture Radar (ISAR), Polarimetric ISAR Imaging and Interpretation

Caner Özdemir

January 9, 2024

Review of Inverse Synthetic Aperture Radar (ISAR), Polarimetric ISAR Imaging and Interpretation

Caner Özdemir
Department of Electrical-Electronics Engineering
Mersin University, Mersin, Türkiye
cozdemir@mersin.edu.tr

Abstract—In this work, a brief but a complete review of Inverse Synthetic Aperture Radar (ISAR) imaging theory is given and the usage of polarimetric imaging concepts in ISAR imaging is shared. First, a very quick summary of ISAR imaging concept is revisited to highlight the key parameters of ISAR imaging such as the geometry, the formulation and the resolution metrics. Then, an example of two-dimensional ISAR image is shared. In the second part of the paper, one of the most comprehensive research topics of ISAR imaging that is polarimetric ISAR is being covered. First, the aspects of polarimetric data collection are revisited. Then, Pauli decomposition technique and its usage in ISAR images are explained. Then, an example of polarimetric ISAR image is provided to together with the polarimetric interpretation of the resultant image.

Keywords—ISAR, radar imaging, radar polarimetry, Pauli decomposition

I. INTRODUCTION

Inverse synthetic aperture radar (ISAR) is a useful and robust signal processing method for displaying moving targets in range-Doppler (or range and cross-range) spaces [1-3]. An ISAR image has the capability of successfully pinpointing the main scattering regions (hot points); i.e., scattering centers on the target that lead to detection and classification of the target [1-5]. Therefore, ISAR images are usually exploited for target detection, automatic target classification (ATC) and recognition (ATR) applications. In the general use of ISAR, the radar antenna is usually excited with a selected linear polarization, either vertical or horizontal. The usage of polarization diversity in ISAR images provide the possibility of extracting more features from the ISAR images such as single/multi-bounce mechanism in junction with the structural feature of the target's sub-parts. Such an information will be so useful that it will increase the accuracy of detection and classification of the target [5-8].

The organization of the paper is as follows: In the next section, the conventional ISAR imagery theory revisited with a 2D simulated ISAR image example of an F-15 airplane model. In Sec. III, the usage of polarimetry in ISAR imaging is given with the explanations of polarization scattering matrix and the polarization scattering decomposition technique of Pauli. Furthermore, co-polarization, cross-polarization and the Pauli ISAR images of a Leopard tank model is provided to better demonstrate the effectiveness of radar polarimetry in ISAR images. The last section is devoted to concluding remarks.

II. REVIEW OF ISAR IMAGING

A. ISAR Geometry and the formulation

On contrary to SAR application, ISAR generally refers to the case when radar platform is stationary while the target is in motion as illustrated in Fig. 1. While the range dimension is resolved by the finite frequency bandwidth of the transmitted waveform, the cross-range dimension is resolved by collecting the back-scattered radar signal from different look-angle of the target as shown in Fig.1.
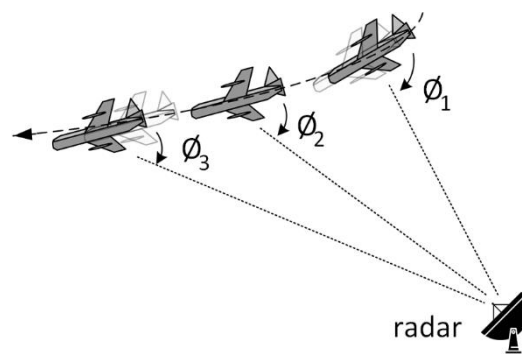

Fig.1. ISAR geometry for imaging

Therefore, this collection provides two-dimensional (2D) data set that can be interpreted to be displayed in the spatial-frequency domains; say, k_x and k_y as demonstrated in Fig. 2. If the backscattered electric-field data were collected within a finite frequency bandwidth; B and within a finite width of look-angles; Ω; then, the resultant 2D raw data generally occupy a non-uniform grid in the $k_x - k_y$ plane as shown in Fig. 2a. Then, the 2D ISAR image of the target can be obtained by taking the following 2D Inverse Fourier integral

$$ISAR(x,y) =$$
$$\frac{1}{\kappa \cdot \Omega} \int_{\phi_1}^{\phi_2} \int_{k_1}^{k_2} \{E_s(k,\phi)\} e^{j2k\cos\phi \cdot x} e^{j2k\sin\phi \cdot y} dk\, d\phi \qquad (1)$$

where $\kappa \triangleq k_2 - k_1$ is the spatial frequency bandwidth and $\Omega \triangleq \phi_2 - \phi_1$ is the angular width while gathering the backscattered electric-field signal. If κ and Ω are not small enough to make the data occupation grid on the $k_x - k_y$ plane rectangular; then the integral in Eqn. (1) should be taken by either direct integration procedures or using a discrete Fourier transform (DFT) based integration after applying a polar reformatting technique [1].

B. ISAR formulation (Small Angles, narrow bandwidth)

If both κ and Ω are appropriately small; the data grid in $k_x - k_y$ space approaches to an equally-spaced linear one as shown in Fig. 2b .This situation makes it possible to make use of fast inverse Fourier transform (IFFT) in forming the ISAR image. Supposing that backscattered electric field from a target can be approximately presented as the sum of scattering from a finite number of single point scatterers, called scattering centers, on the target as

$$E_s(k, \phi) \cong \sum_{i=1}^{K} A_i \cdot \exp\left(-j2\vec{\boldsymbol{k}} \cdot \vec{\boldsymbol{r}}_i\right) \qquad (2)$$

where A_i is the amplitude of the back-scattered signal, $\vec{\boldsymbol{k}}$ is the vector wave number in the propagation direction, $\vec{\boldsymbol{r}}_i = x_i \cdot \hat{\boldsymbol{x}} + y_i \cdot \hat{\boldsymbol{y}}$ is the displacement vector from origin to the location of the ith scattering center. Then, the small-bandwidth small-angle ISAR image can then be approximately calculated as [1]

$$ISAR(x, y) \cong \iint_{-\infty}^{\infty} \sum_{i=1}^{K} A_i \cdot \exp\left(-j2\vec{\boldsymbol{k}} \cdot \vec{\boldsymbol{r}}_i\right) \cdot \exp(j2\pi\alpha x) \cdot \exp(j2\pi\gamma y) \, d\alpha \, d\gamma \qquad (3)$$

where $\alpha = 2f/c$ and $\gamma = (2f_0\phi/c)$ in which f, f_0, and c stand for frequency, center frequency and the speed of light, respectively. The integral in (3) can be conveniently calculated by the practical usage of DFT thanks to nearly uniform data grid on the $k_x - k_y$ plane.


(a)

(b)
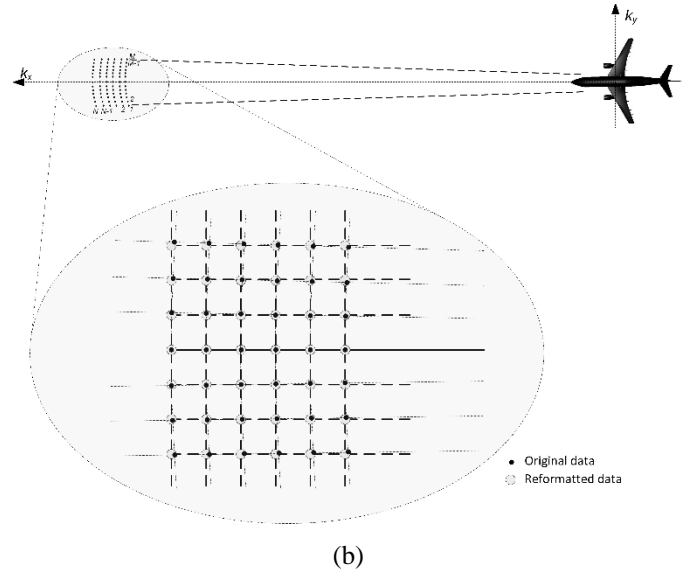
Fig. 2. Collection of ISAR raw data in Fourier space for the monostatic case (2D case), (a) general case, (b) narrow-bandwidth and small-angle case.

C. Resolutions in ISAR image

One of the most important parameters that define the quality of an ISAR image is the resolutions in range and cross-range dimensions. The range resolution is exactly the same as in any radar application as

$$\Delta x = \frac{c}{2B} \qquad (4)$$

where B is the total bandwidth of the radar waveform. The cross-range resolution can be readily obtained from

$$\Delta y = \frac{c}{2f_0\Omega} = \frac{\lambda_0}{2\Omega} \qquad (5)$$

where λ_0 is the center wavelength of the transmitted waveform. The detailed derivation of resolution formulas can be found in [1].

D. 2D ISAR imaging example

The demonstration of 2D ISAR imaging concept is accomplished over an F-15 fighter model whose CAD file can be viewed in Fig. 3a.

To calculate the backscattered electric field from this fighter model, high-frequency electromagnetic scattering simulator tool of PREDICS was used [9,10]. The backscattered electric field were collected for frequencies between $7.625\ GHz$ and $8.367\ Ghz$ for a total of 90 discrete frequencies and from $42.31°$ to $47.62°$ for 90 distinct azimuth angles at the constant elevation angle of $\theta = 105°$. This selection of frequencies and look-angles provide the same range and cross-range resolutions of 20 cm each that can be readily calculated from Eqns. (4) and (5). The electromagnetic solver simulation was carried out for the vertical, vertical (VV) polarization of the transmitted and the reflected waves, respectively. After the PREDICS simulation, a 90×90, 2D multi-frequency multi-aspect backscattered field data were obtained. At the last step, the 2D IFT of the collected
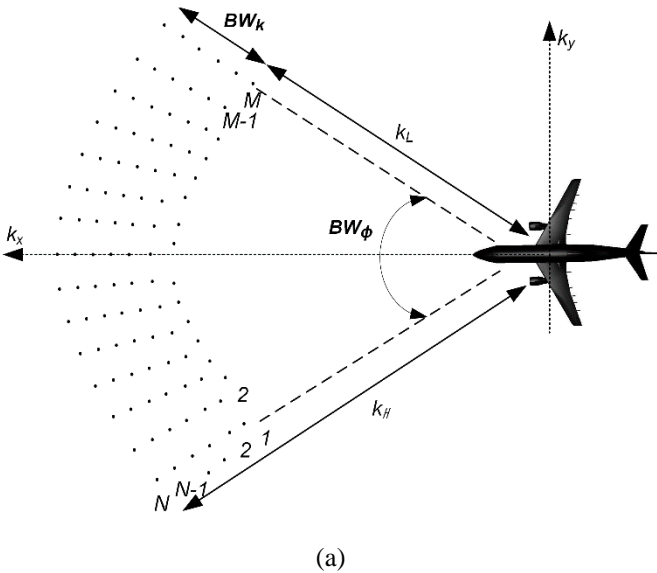
data was taken to form the ISAR image for the VV polarization are shown in Fig. 3b.
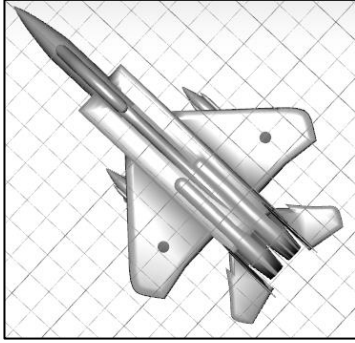
(a)
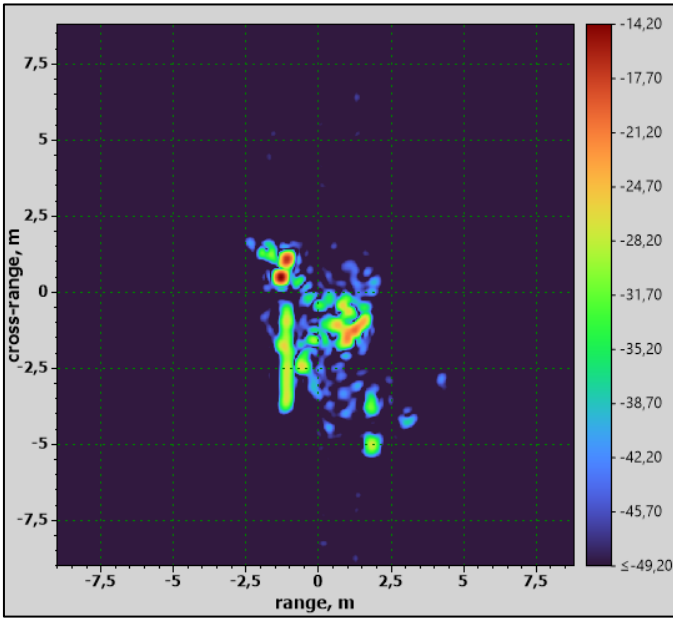
(b)

Fig. 3. (a) F-15 fighter jet model, (b) 2D monostatic ISAR image at X-band for the look angle of ($\theta = 80°, \phi = 45°$) [VV polarization case]

III. POLARIMETRY IN ISAR IMAGING

In the conventional ISAR usage, ISAR receivers capture mono-polarization backscattered field such that only the amplitude information of the image signatures is used for recognition and classification of targets [4-8]. On the other hand, vastly changing image signatures, caused by complex-shaped platforms such as helicopters and tanks need further interpretation in terms of the scattering characteristics. Therefore, the use of radar polarimetry in ISAR imaging can provide some important insights to these scattering phenomena such that the sub-sections of these complex platforms can be identified for much better classification [4].

A. Polarization scattering matrix

Any backscattering from an object at far-field can be fully designated by the 2×2 polarization scattering matrix [S] as the following:

$$\vec{E}^s = \frac{e^{-jkR}}{R}[S]\vec{E}^i \qquad (6)$$

Here, $\vec{E}^s$ and $\vec{E}^i$ are the complex scattered and transmitted (or incident) electric field vectors. If [S] is measured in linear polarization (LP) basis (i.e., H and V); then it can be represented as the following [4]:

$$\begin{bmatrix} E_H^r \\ E_V^r \end{bmatrix} = \frac{e^{-jkR}}{R}\begin{bmatrix} S_{HH} & S_{HV} \\ S_{VH} & S_{VV} \end{bmatrix}\begin{bmatrix} E_H^t \\ E_V^t \end{bmatrix} \qquad (7)$$

where E_H^r and E_V^r stands for the backscattered horizontal and vertical electric fields, respectively.

B. Pauli Decomposition and applications to ISAR images

To express the polarization scattering with the basis of known canonical structures' scattering responses, coherent decompositions techniques such as Pauli, Cameron, and Krogager functions can be conveniently utilized [4, 11, 12].

In the Pauli decomposition technique, [S] is represented with so-called the Pauli basis matrices of Ψ_p. The Pauli basis of $[S]_a, [S]_b, [S]_c$, and $[S]_d$ is presented by the following 2×2 matrices for HH, HV, VV, and VH polarizations, respectively as

$$[S]_a = \sqrt{2}\begin{bmatrix} 1 & 0 \\ 0 & 1 \end{bmatrix}, \qquad [S]_b = \sqrt{2}\begin{bmatrix} 1 & 0 \\ 0 & -1 \end{bmatrix}$$
$$[S]_c = \sqrt{2}\begin{bmatrix} 0 & 1 \\ 1 & 0 \end{bmatrix}, \qquad [S]_d = \sqrt{2}\begin{bmatrix} 0 & -1 \\ 1 & 0 \end{bmatrix}. \qquad (8)$$

Then, the Ψ_P can then be stated with these three orthogonal matrices as $\Psi_P = \{[S]_a, [S]_b, [S]_c\}$. With this set-up, [S] can then be expressed in terms of Pauli decomposition bases as

$$[S] = \begin{bmatrix} S_{HH} & S_{HV} \\ S_{VH} & S_{VV} \end{bmatrix} = \alpha[S]_a + \beta[S]_b + \gamma[S]_c \qquad (9)$$

where $\alpha = (S_{HH} + S_{VV})/\sqrt{2}$, $\beta = (S_{HH} - S_{VV})/\sqrt{2}$, and $\gamma = \sqrt{2}S_{HV}$ are are the complex factors that resemble to the weights of the associated basis matrix.

The $[S]_a$ with $S_{HH} = S_{VV}$ and $S_{HV} = S_{VH} = 0$ can be interpreted as the scattering matrix of an "single-bounce" or "odd-bounce" scatterer caused probably by spheres, flat surfaces and trihedral corner reflectors. The $[S]_b$ includes 180° phase difference between the co-polarized terms and corresponds to the scattering matrix of a dihedral along the look direction. This indicates "double-bounce" or "even-bounce" scattering similar to the one observed from dihedral corner reflectors. The $[S]_c$ corresponds to the scattering matrix of a diplane rotated 45° about the radar's look direction. This term is occasionally associated with "volume scattering" such as from vegetation, forest canopy or from even-bounce objects with 45°orientation.

(a)

(b)

(c)

(d)
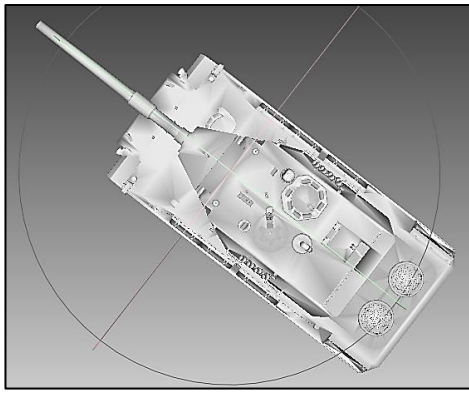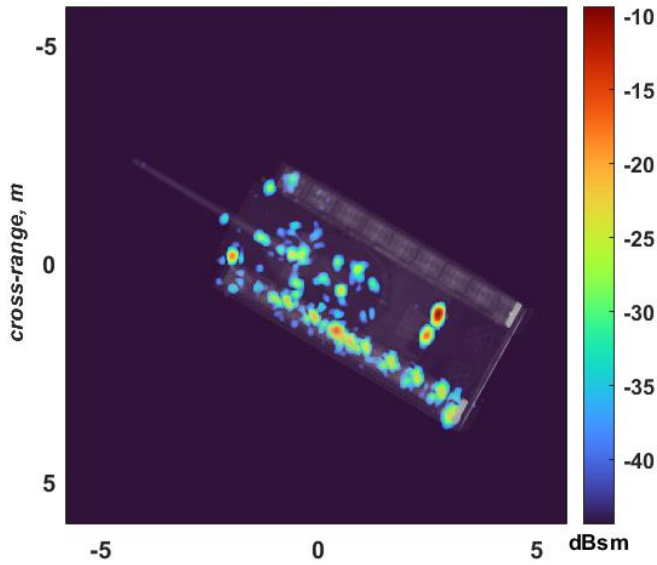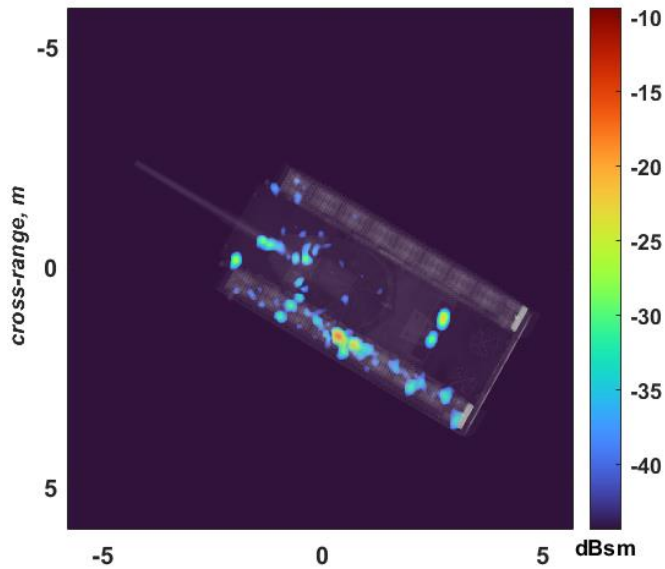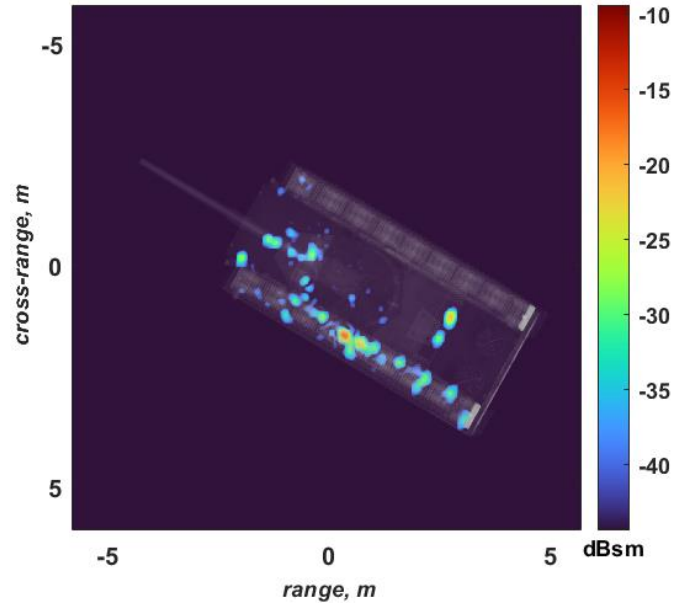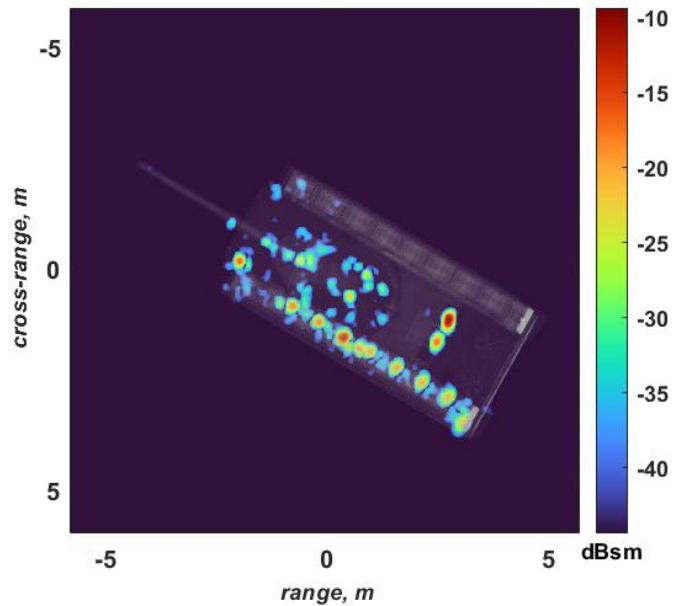
(e)

Fig. 4. (a) Tank model, (b) VV-pol ISAR image, (b) VH-pol ISAR image, (c) HV-pol ISAR image, (d) HH-pol ISAR image

C. Polarimetric ISAR Example

Polarimetric ISAR imaging concept is demonstrated by a complex target that is a model of Leopard tank whose CAD file can be viewed in Fig. 4a. The electromagnetic monostatic backscattering simulation was accomplished by the PREDICS tool [4,10,13]. The fully polarimetric backscattered electric field were collected at the X-bant for frequencies between $11.2\ GHz$ and $12.79\ Ghz$ for a total of 128 discrete frequencies and from $26.18°$ to $33.76°$ for 128 distinct azimuth angles at the constant elevation angle of $\theta = 75°$. After applying the ISAR imaging

steps, the single-polarization ISAR images were attained as depicted in Figs. 4b, c, d, and e for the VV, VH, HV, and HH polarizations, respectively. The scattering mechanism differences can be easily viewed from these four LP polarization images. Although ISAR images for different polarizations looks similar to each other generally, one can observe many discrepancies in the scattering centers due to different scattering mechanisms sensitive to different polarization excitations.
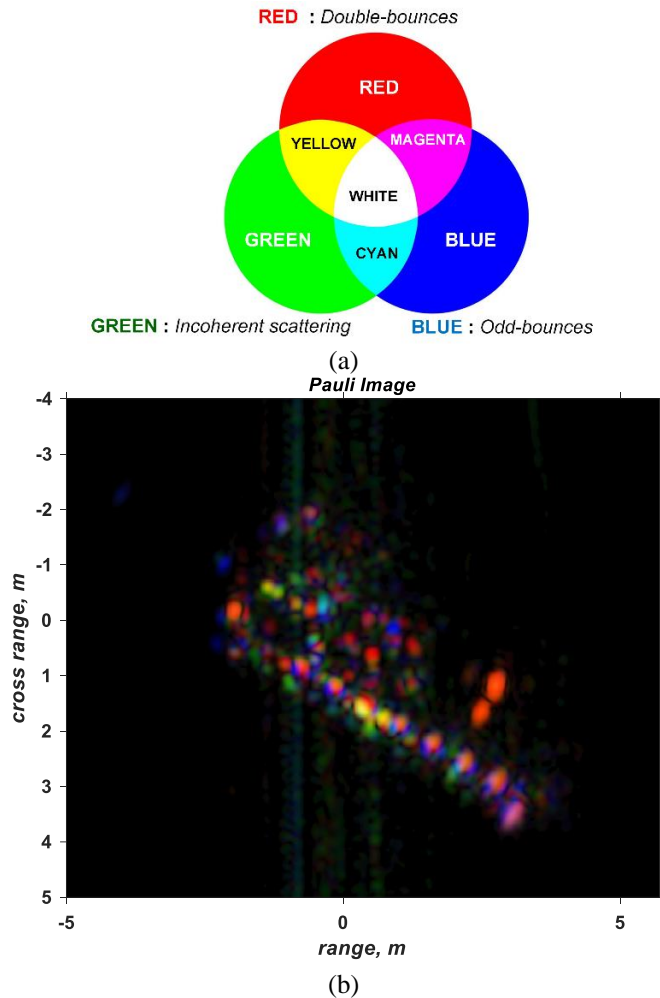

Fig. 5. (a) Pauli RBG color palette, (b) Pauli ISAR image of the tank model

Lastly, the Pauli ISAR image of the tank model was constructed as given in Fig. 5a based on RBG color coding given in Fig. 5b. There happened to be countless scattering phenomenon obtained in this Pauli ISAR image. Only some dominant ones are explained as the followings: Towards the back of the tank, two turret storage bins provided double-bounce mechanisms as they acted like dihedrals. Hence, the echo from this part appeared as red in the resultant Pauli image. On various parts of the tank, many single-bounce echoes have occurred as they showed up as blue color signatures in Fig. 5b. We can also observe some green and yellow color signatures that represent many consecutive multi-bounces with complex scattering mechanisms occur on top of each other. Once the scattering type

is decided by the help of Pauli ISAR images, it yields better accurate identification and classification procedure based on the knowledge of different scattering mechanisms on the target.

IV. Conclusion

In this work, a brief review of ISAR imaging concept was given together with a 2D ISAR imaging example. Then, the usage of radar polarimetry was shared with its application to ISAR imagery. The formulation of the Pauli decomposition, one of the most popular coherent decomposition techniques, was explained. Then, a polarimetric ISAR imaging example applied to a tank model was given. It has been demonstrated that the use of polarimetric diversity would give important insights in characterization of different scattering mechanism off the target that definitely contribute more accurate identification and classification of the target.

References

[1] C. Özdemir, Inverse Synthetic Aperture Radar Imaging with MATLAB Algorithms, Second Edition, John Wiley & Sons, April 2021, Hoboken, New Jersey. *(references)*

[2] K. Ouchi, "Recent trend and advance of synthetic aperture radar with selected topics", Remote Sens., vol. 5, no. 2, pp. 716-807, Feb. 2013.

[3] R. Bhalla and Hao Ling, "A fast algorithm for signature prediction and image formation using the shooting and bouncing ray technique," Proceedings of IEEE APS International Symposium and URSI National Radio Science Meeting, Seattle, WA, USA, 1994, pp. 1990-1993 vol.3.

[4] Ş. Demirci, Ö. Kirik and C. Özdemir, "Interpretation and Analysis of Target Scattering from Fully Polarized ISAR Images Using Pauli Decomposition Scheme for Target Recognition," IEEE Access, vol. 8, pp. 155926-155938, 2020.

[5] J. van Zyl and Y. Kim, Synthetic Aperture Radar Polarimetry, Hoboken, NJ, USA:Wiley, 2011.

[6] S. W. Chen, X. S. Wang, S. P. Xiao and M. Sato, "Advanced polarimetric target decomposition" in Target Scattering Mechanism in Polarimetric Synthetic Aperture Radar, Singapore: Springer, pp. 43-106, 2018.

[7] M. Duquenoy, J. P. Ovarlez, L. Ferro-Famil, E. Pottier and L. Vignaud, "Scatterers characterisation in radar imaging using joint time-frequency analysis and polarimetric coherent decompositions", IET Radar Sonar Navigat., vol. 4, no. 3, pp. 384-402, Jun. 2010.

[8] S. R. Cloude and E. Pottier, "A review of target decomposition theorems in radar polarimetry", IEEE Trans. Geosci. Remote Sens., vol. 34, no. 2, pp. 498-518, Mar. 1996.

[9] C. Özdemir, B. Yılmaz, and Ö. Kırık, "pRediCS: A new GO-PO based ray launching simulator for the calculation of electromagnetic scattering and RCS from electrically large and complex structures," Turkish J. of Electrical Engineering & Computer Sciences, vol. 22, pp. 1255–1269, 2014.

[10] https://www.predicsrcs.com/, accessed on July 5th, 2023.

[11] M. Duquenoy, J. P. Ovarlez, L. F. Famil, L. Vignaud, and E. Pottier, "Study of dispersive and anisotropic scatterers behavior in radar imaging using time frequency analysis and polarimetric coherent decomposition" *2006 IEEE Conference on Radar,* Verona, New York, USA (24-27 April 2006), pp. 180-185.

[12] E. Krogager, W. M. Boerner, and S. N. Madsen, "Feature-motivated Sinclair matrix (sphere/diplane/helix) decomposition and its application to target sorting for land feature classification", *Intern. Symp. on Optical Science, Engineering, and Instrumentation*, San Diego, California, USA(27 July-1 August 1997). 3120 (Wideband Interferometric Sensing and Imaging Polarimetry), pp 144-154.

[13] Ö. Kırık, C. Özdemir, "An Accurate and Effective Implementation of Physical Theory of Diffraction to the Shooting and Bouncing Ray Method via PREDICS Tool", *Sigma J Engineering and Natural Science 2019,* vol. 37, issue: 4, 2019.